J Mol Model (2013) 19:1973–1979
DOI 10.1007/s00894-012-1570-5

ORIGINAL PAPER

Theoretical study on electronic spectra and interaction in $[Au_3]$-L-$[Au_3]$ (L = C_6F_6,Ag^+) complexes

Fernando Mendizabal · Richard Salazar

Received: 20 April 2012 / Accepted: 15 August 2012 / Published online: 2 September 2012
© Springer-Verlag 2012

Abstract The electronic structure and spectroscopic properties of $[Au_3(\mu\text{-}C(OEt) = NC_6H_4CH_3)_3]_n$-$(C_6F_6)_m$ and $[Au_3(\mu\text{-}C^2,N^3\text{-}bzim)_3]_n$-$(Ag^+)_m$ were studied at the B3LYP, PBE and TPSS levels. The interaction between the $[Au_3]$ cluster and L (C_6F_6, Ag^+) was analyzed. Grimme's dispersion correction is used for those functionals. Weak π-interactions (Au-C_6F_6) were found to be the main contribution short-range stability in the models; while in the models with Ag^+, an ionic interaction is obtained. The absorption spectra of these models at the PBE level agree with the experimental spectra.

Keywords Electronic spectra · Secondary interaction · Trigold(I)

Introduction

Cyclic trinuclear gold(I) complexes represent an important class of coordination compounds in different areas such as acid-base chemistry, metalloaromaticity, metallophilic bonds, supramolecular assemblies and host/guest chemistry [1–4]. Among the gold(I) complexes reported in the literature, $[Au_3(\mu\text{-}C^2,N^3\text{-}bzim)_3]$ (bzim = 1-benzylimidazolate) and $[Au_3(\mu\text{-}C(OEt) = NC_6H_4CH_3)_3]$ act as bases which form complexes with several electrophiles [5–7]. The electrophiles are Lewis acids which can be organic molecules (C_6F_6, $C_{10}F_8$, TCNQ) [5], polyfunctional clusters of the type $[Hg_3(O\text{-}C_6F_4)_3]$ [6], and heavy metal cations (Ag^+ and Tl^+) [7]. All the compounds mentioned above show interesting bonding, optoelectronic, and luminescence properties [2].

In particular, $[Au_3(\mu\text{-}C(OEt) = NC_6H_4CH_3)_3]$ forms deeply colored charge-transfer stacks with C_6F_6 [2, 6]. In complexes that include organic molecules, the contacts possibly reflect the presence of weak polyhapto-π interactions. Also, these adducts display an intense room-temperature photoluminescence in the UV-visible range [6]. On the other hand, $[Au_3(\mu\text{-}C^2,N^3\text{-}bzim)_3]$-$\{Ag\}^+$ displays visible luminescence consistent with the extended-chain structures observed [7]. In general, the donor-acceptor interaction invokes dispersion and electrostatic intermolecular forces that probably add to the stability of the adducts [8].

In the literature, the aurophilic attraction and the spectroscopic properties of $[Au_3(MeN = COMe)_3]_n$ (n=1-4) [9], $[Au_3(CH_3N = COCH_3)_3]\cdot\{2,4,7\text{-trinitro-9-fluorenone}\}$ [10] and $[Hg_3(O\text{-}C_6F_4)_3]\cdot\{benzene\}$ [11] were studied at the MP2 (second-order Møller-Plesset perturbation theory) and density functional theory (B3LYP and PBE (Perdew-Burke-Ernzerhof)) levels. Theoretical calculations at the MP2 level are in agreement with experimental geometries and aurophilic attraction, and to a lower extent for PBE. The absorption spectra of these gold(I) complexes were calculated by the single excitation time-dependent (TD) density functional method. The theoretical results agree with the experimental results [12–14].

In order to test these intermolecular forces and their effect on properties such as electronic spectra, we have performed a theoretical study based on the DFT at B3LYP, PBE and TPSS levels using the clusters of the type $[Au_3(\mu\text{-}C(OEt) = NC_6H_4CH_3)_3]_n$-$(C_6F_6)_m$ and $[Au_3(\mu\text{-}C^2,N^3\text{-}bzim)_3]_n$-$(Ag^+)_m$. In addition, we have included the effect of dispersion for the first cluster at the DFT level. We propose to study the effect of several

F. Mendizabal · R. Salazar
Departamento de Química, Facultad de Ciencias,
Universidad de Chile,
Casilla 653,
Santiago, Chile

F. Mendizabal (✉)
Center for the Development of Nanoscience and Nanotechnology,
CEDENNA,
Santiago, Chile
e-mail: hagua@uchile.cl

complexes and how their interactions can influence the spectroscopic absorption properties. To our knowledge, so far no systematic TD-DFT investigations have been made on these systems.

Models and methods

The $[Au_3(\mu\text{-}C(OEt) = NC_6H_4CH_3)_3]_n\text{-}(C_6F_6)_m$ (1,2) and $[Au_3(\mu\text{-}C^2,N^3\text{-}bzim)_3]_n\text{-}(Ag^+)_m$ (3,4) models used in this study are depicted in Fig. 1. The geometries were fully optimized at the scalar quasi-relativistic B3LYP, PBE [15] and TPSS (Tao-Perdew-Staroverov-Scuseria) [16] levels in the gas phase. Regarding these methods, PBE and TPSS have been used in the study of weak interactions [17–19]. These are the best available functionals without parameters fitted to experimental data. However, none of the existing functionals are optimal for evaluating the van der Waals and dispersion interactions [20]. In particular, these weak interactions are important for systems with hexafluorobenzene (1,2). Due to this reason, Grimme's dispersion correction is used for those functionals for which are available, and its use is indicated by appending "DFT-D3" to the acronym of the density functional [21–23]. The DFT-D3 methodology is based on the total energy is given by

$$E_{DFT-D3} = E_{KS-DFT} - E_{disp}, \quad (1)$$

where $E_{KS\text{-}DFT}$ is the self-consistent Kohn-Sham energy as obtained from the chosen functional and E_{disp} is a dispersion correction given by the sum of two- and three-body energies,

$$E_{disp} = E^{(2)} + E^{(3)}, \quad (2)$$

with the $E^{(2)}$ and $E^{(3)}$ terms defined as

$$E^{(2)} = \sum_{AB} \sum_{n=6,8,10,.....} S_n \frac{C_n^{AB}}{r_{AB}^n} f_{d,n}(r_{AB}) \quad (3)$$

$$E^{(3)} = \sum_{ABC} f_{d,3}(r_{ABC}) E^{ABC} \quad (4)$$

In the Eq. 3, the first sum runs all atom pair, C_n^{AB} denotes the *n*th-order dispersion coefficient for atom pair AB, r_{AB} is their interatomic distance, and $f_{d,n}$ is damping function. On the other hand, in Eq. 4 the sum is over all atom triples ABC in the system and E^{ABC} is nonadditive dispersion term as derived from third-order perturbation theory for three atoms ABC; $f_{d,3}$ is damping function.

The excitation energies were obtained at the PBE level by means of the time-dependent perturbation theory approach (TD-DFT) [24, 25], which is based on the random-phase approximation (RPA) method [26]. Single point calculations of geometry model 1–4 were simulated to study the excitation spectra. The TD-DFT calculations do not evaluate the spin-orbit splitting, and the values are averaged.

The calculations were done using the Turbomole package (version 6.2) [27]. For Au and Ag, the 19 valence-electron (VE) quasi-relativistic (QR) pseudo-potential (PP) of Andrae et al. [28] was employed. We used two *f*-type polarization functions on gold (α_f=0.20, 1.19) and silver (α_f = 0.22,1.72) [29]. Also, the C, N, O and F atoms were treated through PPs, using double-zeta basis sets with the addition of one d-type polarization function [30]. For the H atom, a double-zeta basis set plus one p-type polarization function was used [31]. All geometry calculations have been obtained used the efficient resolution of identity (RI) [32].

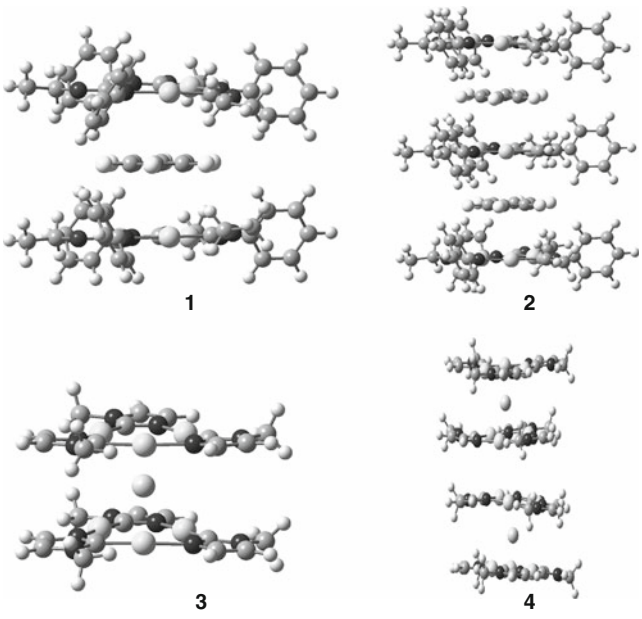

Fig. 1 The models $[Au_3(\mu\text{-}C(OEt) = NC_6H_4CH_3)_3]_2\text{-}(C_6F_6)$ (1), $[Au_3(\mu\text{-}C(OEt) = NC_6H_4CH_3)_3]_3\text{-}(C_6F_6)_2$ (2), $[Au_3(\mu\text{-}C^2,N^3\text{-}bzim)_3]_2\text{-}(Ag^+)$ (3) and $[Au_3(\mu\text{-}C^2,N^3\text{-}bzim)_3]_2\text{-}(Ag^+)$ (4)

Results and discussion

Molecular geometry and interaction energy

We have fully optimized the geometries for the models 1–4. Tables 1 and 2 show the main parameters, together with relevant experimental structural data. The theoretical results are in agreement with the experimental data when the $[Au_3(\mu\text{-}C(OEt) = NC_6H_4CH_3)_3]\cdot\{C_6F_6\}$ complex is compared at the B3LYP, PBE and TPSS levels. It is seen that the structural parameters do not change substantially when going from model 1 to model 2. In both models it is possible to see that the Au-Au intramolecular distance is short by

Table 1 Main geometric parameters of the $[Au_3(\mu\text{-}C(OEt) = NC_6H_4CH_3)_3]_n\text{-}(C_6F_6)_m$ complexes (distances in pm and angles in degrees)

Complexes	Method	Au-Au[a]	AuC[b]	AuC[c]	AuN	CF	NAuC°	AuAuAu°
$[Au_3(\mu\text{-}C(OEt) = NC_6H_4CH_3)_3]_2\text{-}C_6F_6$ (1)	B3LYP	339.3	201.0	376.0	210.0	133	178.8°	59.73°
	PBE	334.0	199.0	360.9	209.0	133	178.8°	59.68°
	TPSS	332.1	200.0	368.8	208.0	133	178.5°	59.99°
	B3LYP-D3	345.3	203.7	345.0	212.2	133	174.8°	60.00°
	PBE-D3	337.8	201.5	334.9	210.9	132	175.4°	60.00°
	TPSS-D3	337.1	201.8	331.4	210.6	132	175.8°	60.00°
$[Au_3(\mu\text{-}C(OEt) = NC_6H_4CH_3)_3]_3\text{-}(C_6F_6)_2$(2)	B3LYP	338.8	201.5	380.7	209.8	133	179.1°	59.99°
	PBE	334.5	199.3	360.4	208.5	134	178.6°	59.95°
	TPSS	332.3	200.0	368.3	208.0	134	178.3°	59.99°
	B3LYP-D3	345.2	203.6	350.1	211.5	133	175.3°	60.00°
	PBE-D3	336.9	201.4	334.2	210.8	132	174.3°	60.00°
	TPSS-D3	332.9	201.5	332.0	210.6	133	175.5°	60.00°
$[Au_3(\mu C(OEt) = NC_6H_4CH_3)_3]_\infty \cdot \{C_6F_6\}$	Exp.	349.1	199.7	356.5	205.0	133	175.2°	60.00°

[a] Au—Au intramolecular distance

[b] Au—C distance C(OEt) = $NC_6H_4CH_3$ groups

[c] Au—C distance C_6F_6

three DFT methods compared to the experimental structure. Also, the Au-C (C_6F_6) distances show a weak attraction at the DFT levels which is longer than the experimental value (356.5 pm). The latter results should be analyzed with caution, since DFT calculations do not describe appropriately the van der Waals (dispersion) attractions, although DFT can occasionally reproduce the van der Waals distance [20]. On the other hand, this distance decreases, increasing the interaction, once we include the DFT-D3 dispersion correction. The effect on other geometric parameters is very small.

On the other hand, the silver complex shown in model 3 gives distances close to the experimental value regardless of the DFT method (see Table 2). For example, the Au-Ag experimental distance is 281.1 pm and the theoretical values are between 284.5 and 296.2 pm. However, in model 4, which includes a second cluster, there are Au-Au intermolecular interactions. Only with the PBE method was it possible to obtain an Au-Au intermolecular contact at 333.0 pm. The experimental value is 319.0 pm. B3LYP and TPSS methods for such intermolecular interaction is not taken into account because the Au-Au distances are between 1319.0 pm and 1400.0 pm, respectively. These are extremely long distances. The results have not been included in Table 2.

We have estimated the interaction energies $[Au_3(\mu\text{-}C(OEt) = NC_6H_4CH_3)_3]_n\text{-}(C_6F_6)_m$ and $[Au_3(\mu\text{-}C^2,N^3\text{-}bzim)_3]_n\text{-}(Ag^+)_m$ for models 1–4 with counterpoise correction (CP) for the basis-set superposition error (BSSE). The results are shown in Table 3. We obtain a shorter Au-C (C_6F_6) equilibrium distance for models 1 and 2, between 368.3 and 380.7 pm, with interaction energies between 44.1 and 86.1 kJ mol^{-1}, respectively; for clusters without including the dispersion term. The electrostatic and induction contributions would still be there and their magnitudes are between 2.0 and 7.2 kJ mol^{-1}. One may expect that the inclusion of *f* functions on gold atoms should reduce the BSSE. This situation changes drastically once we have included the DFT-D3. The distances Au-C (C_6F_6) decrease,

Table 2 Main geometric parameters of the $[Au_3(\mu\text{-}C^2,N^3\text{-}bzim)_3]_n\text{-}(Ag^+)_m$ complexes (distances in pm and angles in degrees)

Complexes	Method	Au-Ag	Au-Au[a]	Au-Au[b]	Au-C[c]	Au-N	NAuC°	AuAuAu°
$[Au_3(\mu\text{-}C^2,N^3\text{-}bzim)_3]_2\text{-}Ag^+$ (3)	B3LYP	296.2	354.0	–	201.0	208.0	174.8°	59.99°
	PBE	286.7	350.5	–	199.0	206.0	175.3°	59.99°
	TPSS	284.5	348.7	–	200.0	206.0	175.7°	59.99°
$[Au_3(\mu\text{-}C^2,N^3\text{-}bzim)_3]_4\text{-}(Ag^+)_2$ (4)	PBE	286.8	350.0	333.0	199.0	206.0	174.8°	59.99°
$[Au_3(\mu\text{-}C^2,N^3\text{-}bzim)_3]_\infty \cdot \{Ag^+\}$	Exp.	281.1	326.8	319.0	199.7	203.0	173.2°	59.6°

[a] Au—Au intramolecular distance

[b] Au—Au intermolecular distance

[b] Au—C distance $\mu\text{-}C^2,N^3$ -bzim groups

Table 3 Intermolecular distance Au-C (pm), Au-M and interaction energies, $V(R_e)$, in kJ mol^{-1} by complexes (1–4) with counterpoise (CP) correction

System	Method	Au-X[a]	$V(R_e)$	Au-C pair
$[Au_3(\mu\text{-}C(OEt) = NC_6H_4CH_3)_3]_2\text{-}C_6F_6$ (1)	B3LYP	376.0	−44.1	−3.7
	PBE	360.9	−86.1	−7.2
	TPSS	368.8	−69.0	−5.8
	B3LYP-D3	345.0	−108.1	−9.0
	PBE-D3	334.9	−147.8	−12.3
	TPSS-D3	331.4	−164.8	−13.7
$[Au_3(\mu\text{-}C(OEt) = NC_6H_4CH_3)_3]_3\text{-}(C_6F_6)_2$ (2)	B3LYP	380.7	−45.2	−1.8
	PBE	360.4	−85.0	−3.5
	TPSS	368.3	−69.5	−2.9
	B3LYP-D3	345.2	−252.5	−10.5
	PBE-D3	334.2	−281.8	−11.7
	TPSS-D3	332.9	−323.6	−13.5
$[Au_3(\mu\text{-}C^2,N^3\text{-}bzim)_3]_2\text{-}Ag^+$ (3)	B3LYP	296.2	−478.3	
	PBE	286.7	−645.9	
	TPSS	284.5	−590.3	
$[Au_3(\mu\text{-}C^2,N^3\text{-}bzim)_3]_4\text{-}(Ag^+)_2$ (4)	PBE	286.8	−571.4	

[a]Au-X intramolecular distance when X is C_6F_6 (1,2), Ag (3,4)

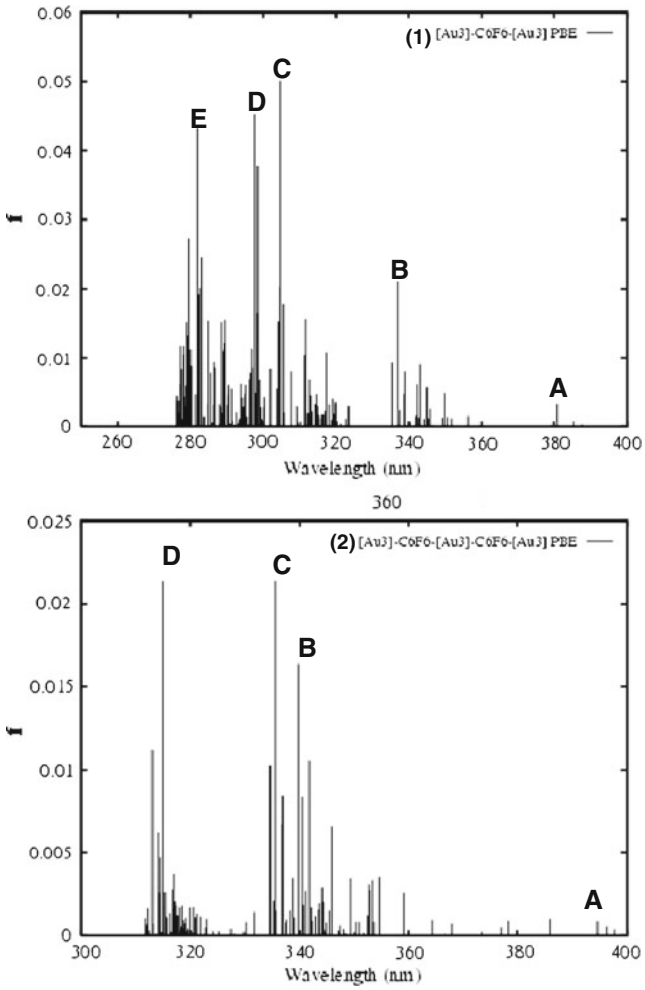

Fig. 2 Calculated electronic PBE spectra for models 1 and 2

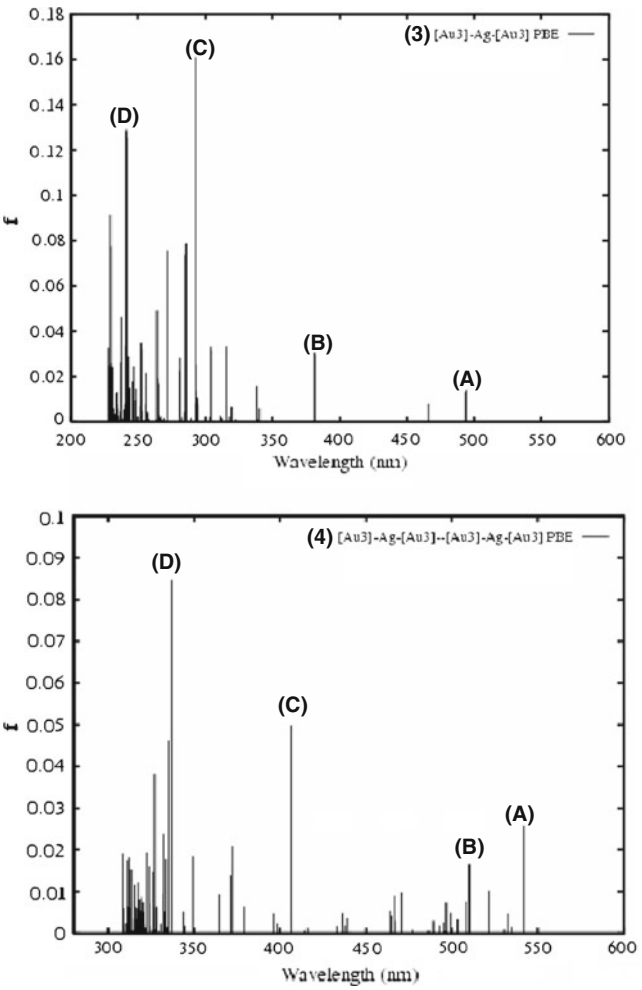

Fig. 3 Calculated electronic PBE spectra for models 3 and 4

Table 4 TD-DFT/PBE-D3 singlet-excitation calculations for $[Au_3(\mu\text{-}C(OEt) = NC_6H_4CH_3)_3]_n\text{-}(C_6F_6)_m$

Complexes	λ_{calc}	f[a]	Contributions[b]	Transition type
$[Au_3(\mu\text{-}C(OEt) = NC_6H_4CH_3)_3]_2\text{-}C_6F_6$ (1)	395 (A)	0.0033	259a→262a (99%)	MLCT (d→π*)
	337 (B)	0.0210	258a→263a (32%)	MMCT (d+π*→d+π*)
			258a→265a (25%)	MMLCT (d+π*→d+π*)
			259a→264a (15%)	MMLCT (d→d*+π*)
	305 (C)	0.0500	259a→270a (17%)	MMLCT (d→d*+π*)
			258a→270a (15%)	MMLCT (d+π*→d+π*)
			261a→271a (13%)	MLCT (dz2+π*→d*+π*)
	298 (D)	0.0450	253a→266a (19%)	MMLCT (d→d*+π*)
			246a→262a (8%)	LLCT (π*→π*)
			247a→262a (7%)	LLCT (π*→π*)
			245a→262a (7%)	MLLCT (d*+π*→π*)
	282 (E)	0.0430	256a→270a (35%)	MMLCT (d*+π*→d*+π*)
			255a→270a (22%)	LMLCT (π*→d*+π*)
$[Au_3(\mu\text{-}C(OEt) = NC_6H_4CH_3)_3]_3\text{-}(C_6F_6)_2$ (2)	395 (A)	0.00086	406a→409a (99%)	MLCT (d→π*)
	340 (B)	0.0163	406a→416a (16%)	MLCT (d→π*)
			404a→414a (13%)	LMLCT (π→d+π*)
			403a→415a (12%)	LMLCT (π*→d+π*)
			403a→412a (11%)	LMLCT (π*→π*)
			404a→416a (9%)	LLCT (π→π*)
	336 (C)	0.0213	403a→414a (31%)	LMLCT (π*→d+π*)
			403a→413a (14%)	LLCT (π→π*)
			405a→414a (14%)	LMLCT (π*→d+π*)
	315 (D)	0.0214	402a→413a (35%)	LLCT (π*→π)
			403a→417a (17%)	LLCT (π*→π*)
			403a→419a (9%)	LLCT (π*→π*)

[a] Oscillator strength

[b] Values are $|coeff.|^2 \times 100$

Table 5 TD-DFT/PBE singlet-excitation calculations for $[Au_3(\mu\text{-}C^2,N^3\text{-}bzim)_3]_n\text{-}(Ag^+)_m$

Complexes	λ_{calc}	f[a]	Contributions[b]	Transition type
$[Au_3(\mu\text{-}C^2,N^3\text{-}bzim)_3]_2\text{-}Ag^+$ (3)	495 (A)	0.0141	157a→160a (100%)	MMCT (π*→6s)
	382 (B)	0.0302	151a→160a (74%)	MMCT (dz2+d→6s)
			150a→160a (23%)	MMCT (dz2+d→6s)
	293 (C)	0.0161	154a→162a (21%)	MMCT (dz2+d*→d)
			155a→161a (17%)	LMMCT (π*+d→π)
			155a→162a (14%)	LMMCT (π*+d→d)
			153a→161a (11%)	MMCT (dz2+dxy*→π)
	241 (D)	0.125	153a→165a (28%)	MMCT (dz2+dxy*→π)
			157a→170a (22%)	MMCT (π*→π*)
$[Au_3(\mu\text{-}C^2,N^3\text{-}bzim)_3]_4\text{-}(Ag^+)_2$ (4)	542 (A)	0.0256	318a→319a (87%)	MMCT (dz2+d→6s)
			314a→319a (4%)	MMCT (π*→6s)
	510 (B)	0.0167	313a→319a (74%)	MMCT (π→6s)
			318a→320a (10%)	MMCT (dz2→6s)
	407 (C)	0.0498	302a→319a (83%)	MMCT (dz2*→6s)
	337 (D)	0.0847	318a→321a (58%)	MMCT (dz2→π)
			292a→319a (30%)	MMCT (dxy+π→6s)

[a] Oscillator strength

[b] Values are $|coeff.|^2 \times 100$

increasing the interaction between both centers. If we consider that each gold interacts with two carbons, we can estimate approximately the energy of each Au-C pair. We can see that there is a strong oscillation depending on the methodology, the pair-wise energies of Au-C interactions are among 9.0 and 13.5 kJ mol^{-1}.

On the other hand, in models 3 and 4 the interaction energies clearly show that the silver generates an ionic interaction with the gold atoms. The interaction energies are between 645.9 and 478.1 kJ mol^{-1}, depending on the method used (see Table 3). This shows clearly a strong bond between the gold core and the silver cation. We can see this fact reflected through the magnitudes of charges of the Ag (+0.80/+0.85) and the Au_3 core (−0.20/-0.15), as obtained with NBO analysis.

Time-dependent (TD) DFT calculations

The experimental UV-visible spectra of these complexes have been reported. That of the $[Au_3(\mu\text{-}C(OEt) = NC_6H_4CH_3)_3]$-$\{C_6F_6\}$ adduct shows enhanced absorption in the 380–550 nm region with a peak maximum at 432 nm and a shoulder at 410 nm, which is indicative of a charge-transfer interaction [6]. On the other hand, the $[Au_3(\mu\text{-}C^2,N^3\text{-}bzim)_3]_2$-$\{Ag^+\}$ complex shows a luminescence spectra at 535 nm (green color at 298º K) [7].

We calculated the allowed spin singlet transition for these complexes, based on the ground state structures of models 1–4 at the PBE-D3 and PDE levels, respectively. Only singlet-singlet transitions were considered in these scalar quasi-relativistic calculations. We consider as allowed transitions those whose oscillator strength is different from zero. The allowed transitions obtained are shown in Figs. 2 and 3 and Tables 4 and 5. We analyze the most important transitions. The active molecular orbitals in electronic transitions at the PBE level are shown in Figs. 4 and 5 for one of the transitions.

$$\left[Au_3(\mu - C(OEt) = NC_6H_4CH_3)_3\right]_n - (C_6F_6)_m(1,2)$$

The electronic structure of the models have been described with several absorption peaks, and the transitions are described in Fig. 2 and summarized in Table 4. In both models (1,2), there is a significant transition at 395 nm (A) which is assigned to individual states of a metal-ligand charge transfer (MLCT). This band is very close to that experimentally obtained at 432 nm.

The bands in models 1 and 2 at 395 nm are composed mainly of the 259a (d) → 262a (π*) and 406a (d) → 409a (π*) transitions, respectively. This band corresponds to MLCT. Thus, the transition involved in this orbital goes from gold core cluster orbitals to antibonding π* of C_6F_6. The active molecular orbitals in the electronic transition are shown in Fig. 4. It is noted that there is no change in the effect on the band of adding a gold cluster and extra C_6F_6 in model 2.

$$\left[Au_3\left(\mu - C^2, N^3 - bzim\right)_3\right]_n - (Ag^+)_m(3,4)$$

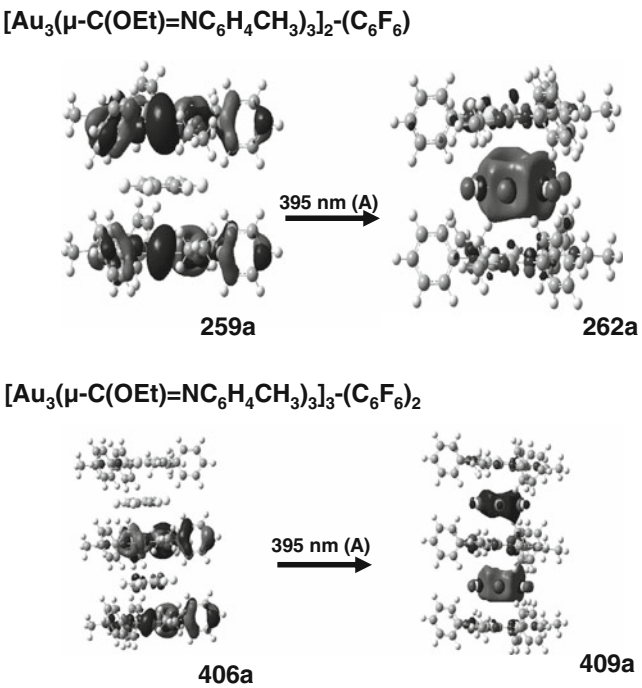

Fig. 4 More important active molecular orbitals in the electronic transitions **a** of models 1 and 2 at the PBE level

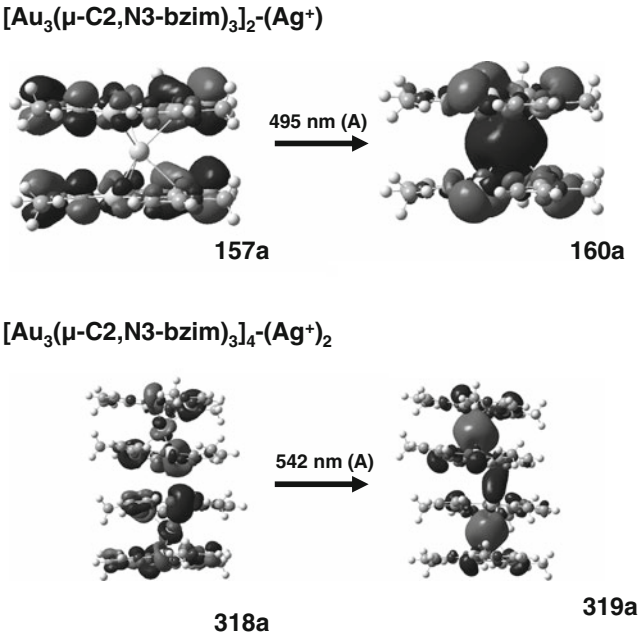

Fig. 5 More important active molecular orbitals in the electronic transitions **a** of models 3 and 4 at the PBE level

For models 3 and 4, we focus on a particular transition, the closest to the experimental band. Thus, a red shift is seen of the main excited bands at 495 to 542 nm (A) when going from model 3 to model 4 (see Fig. 3 and Table 5). The bands are mainly a MMCT, very close to the experimental band at 535 nm. This transition in models 3 and 4 is composed mainly of 157a (π^*) → 160a (6s) (495 nm) and 318a (dz2 + d) → 319a (6s) (542 nm), respectively. These transitions can be understood from the MOs shown in Fig. 5. It is possible to see the transition from the gold core to the 6s orbital of the silver.

Conclusions

This study provides further information on the nature of the gold-carbon(C_6F_6) and gold-silver intermolecular interaction in the $[Au_3(\mu\text{-}C(OEt) = NC_6H_4CH_3)_3]\cdot\{C_6F_6\}$ and $[Au_3(\mu\text{-}C^2, N^3\text{-}bzim)_3]_2\text{-}\{Ag^+\}$ complexes and on their spectroscopic properties. Theoretical calculations at the DFT level are in agreement with experimental geometries and weak π-interactions in $[Au_3(\mu\text{-}C(OEt) = NC_6H_4CH_3)_3]\cdot\{C_6F_6\}$. It has been demonstrated that the origin of such an interaction is dispersion type in the three methods including the DFT-D3 correction of Grimme and co-workers. In the $[Au_3(\mu\text{-}C^2,N^3\text{-}bzim)_3]_2\text{-}\{Ag^+\}$ models, there is a bond of significant ionic character between the gold core and silver. The aim of TD-DFT/PBE calculations was to predict the excitation spectra. The results show a type LMCT in models 1 and 2, with participation of the gold core and C_6F_6 molecule. The $[Au_3(\mu\text{-}C^2,N^3\text{-}bzim)_3]_2\text{-}\{Ag^+\}$ complex was reproduced by models 3 and 4. The spectra at TD-DFT/PBE give very good agreement with the experimental band, with participation of the gold core and Ag (6s).

Acknowledgments This research was financed by Fondo Nacional de Ciencia y Tecnología (FONDECYT) under Project 1100162 (Conicyt-Chile), Project Millennium P07-006-F, and Basal Financing Program Comisión Nacional de Ciencia y Tecnología (CONICYT)-FB0807 (Centro de Nanociencia y Nanotecnología, CEDENNA).

References

1. Omary MA, Rawashdeh-Omary MA, Gonser MWA, Grimes T, Cundari TR (2005) Inorg Chem 44:8200–8210
2. Omary MA, Mohamed AA, Rawashdeh-Omary MA, Facker JP (2005) Coord Chem Rev 249:1372–1381
3. Hayashi A, Olmstead MM, Attar S, Balch AL (2002) J Am Chem Soc 124:5791–5795
4. Omary MA, Kassab RM, Haneline MR, Elbjeirami O, Gabbaï FP (2003) Inorg Chem 42:2176–2178
5. Rawashdeh-Omary MA, Omary MA, Fackler JP (2001) J Am Chem Soc 123:9689–9691
6. Burini A, Fackler JP, Galassi R, Grant TA, Omary MA, Rawashdeh-Omary MA, Pietronic BR, Staples RJ (2000) J Am Chem Soc 122:11264–11265
7. Burini A, Bravi R, Fackler JP, Galassi R, Grant TA, Omary MA, Pietronic BR, Staples RJ (2000) Inorg Chem 39:3158–3165
8. Olmstead MM, Jiang F, Attar S, Balch AL (2001) J Am Chem Soc 123:3260–3267
9. Mendizabal F, Aguilera B, Olea-Azar C (2007) Chem Phys Lett 447:345–351
10. Mendizabal F (2010) Int J Quant Chem 110:1279–1286
11. Mendizabal F, Burgos D, Olea-Azar C (2008) Chem Phys Lett 463:272–277
12. Fernández EJ, Jones PG, Laguna A, López-de-Luzuriaga JM, Monge M, Pérez J, Olmos ME (2002) Inorg Chem 41:1056–1063
13. Mendizabal F, Olea-Azar C (2005) Int J Quant Chem 103:34–44
14. Mendizabal F, Burgos D, Olea-Azar C (2009) Int J Quant Chem 109:477–482
15. Perdew JP, Burke K, Ernzerhof M (1996) Phys Rev Lett 77:3865–3868
16. Tao J, Perdew P, Staroverov VN, Scuseria GE (2003) Phys Rev Lett 91:146401–146403
17. Wang YB, Lin Z (2003) J Am Chem Soc 125:6072–6073
18. Johnson ER, DiLabio GA (2006) Chem Phys Lett 419:333–338
19. Johansson MP, Lechtken A, Schooss D, Kappes MM, Furche F (2008) Phys Rev A 77:053202–053208
20. Johansson MP, Sundholm D, Vaara J (2004) Angew Chem Int Ed Engl 43:2678–2681
21. Grimme S, Antony J, Ehrlich S, Krieg H (2010) J Chem Phys 132:154104, 1–10
22. Hujo W, Grimme S (2011) J Chem Theor Comput 7:3866–3871
23. Grimme S (2012) ChemPhysChem 13:1407–1409
24. Bauernschmitt R, Ahlrichs R (1996) Chem Phys Lett 256:454–464
25. Casida ME, Jamorski C, Casida KC, Salahub DR (1998) J Chem Phys 108:4439–4449
26. Olsen L, Jϕrgensen P (1995) In: Yarkony DR (ed) Modern Electronic Structure Theory, vol 2. World Scientific, River Edge
27. Ahlrichs R, Bär M, Häser M, Horn H, Kölmel C (1989) Chem Phys Lett 162:165–169
28. Andrae M, Heisserman M, Dolg M, Stoll H, Preuss H (1990) Theor Chim Acta 77:123–141
29. Pyykkö P, Runeberg N, Mendizabal F (1997) Chem Eur J 3:1451–1457
30. Bergner A, Dolg M, Küchle W, Stoll H, Preuss H (1993) Mol Phys 80:1431–1441
31. Huzinaga S (1965) J Chem Phys 42:1293–1301
32. Eichkorn K, Treutler O, Öhm H, Häser M, Ahlrichs R (1995) Chem Phys Lett 240:283–289